Characterization of Methane Production of a Páramo Peatbog in Colombia throughout the Holocene

Andrés Camilo Zúniga González

Advisor: Catalina González Arango

Co-Advisor: Adriana Jimena Bernal Giraldo

A dissertation submitted to the Universidad de los Andes

in accordance with the requirements for the degree:

Master in Biological Sciences – Biology Focus

in the Faculty of Sciences,

Department of Biological Sciences

January 2020

Acknowledgments

Introduction

Climate change and its consequences for future generations have been the center of discussion on the current agenda of environment preservation debates; it has mainly focused attention on the role of carbon dioxide (CO_2) as the main contributor to global warming, due to its effects as a greenhouse gas and, mostly, due to its accelerated concentration increase caused by human activities in the last century (1). Nonetheless, CO_2 is not the only, nor the strongest gas involved in the heating process; other greenhouse gases include water vapor (H_2O), nitrous oxide (N_2O), ozone (O_3), chlorofluorocarbons (CFCs), hydrofluorocarbons (HFCs) and methane (CH_4). The latter is particularly relevant because it has a greater global warming potential on short and large timescales compared to the other gases (2–4). As is the case with CO_2, anthropogenic activities currently account for most of atmospheric CH_4; such include livestock raising, fossil fuel extraction and massive rice farming (5). However, biogenic emissions have historically been greater, considering the large sinks of frozen methane stored in the ocean floor, as well as in permafrost soils in the Arctic (6). Among natural sources, wetlands are responsible for 70% of released methane, with an increasing trend of their total input, caused by ice melting, especially in temperate zones. These ecosystems are distributed worldwide and play a significant role in carbon cycling, hence in methanogenesis, thanks to high water availability and rich organic matter content in their soils. In this regard, several studies have measured the contribution of high latitude wetlands; nonetheless, such extensive research is yet to be done in tropical wetlands, even though it has been estimated that their emissions are far larger than temperate ones (7,8).

In light of the above, methane production in wetlands must be strictly conducted under anoxic conditions by some species of Archaea, as the ending step in organic carbon degradation (9). The process by which these anaerobic organisms, known as methanogens, convert carbon compounds into CH_4 can have several pathways, depending on the availability and abundance of certain molecules, like water and carbon-based compounds, and the appropriate environmental conditions, such as temperature and pH. However, two paths prevail among the others, acetotrophy and hydrogenotrophy. Both routes use acetate (CH_3COO^-) and hydrogen molecules (H_2) respectively, as substrates for carbon reduction. Archaea from the genera *Methanosaeta* and *Methanosarcina* use the first one, while hydrogen as reducing agent is more widespread among other methanogen species. As the previous suggests, which way is predominant relies largely on community composition and substrate accessibility; nevertheless, some environmental conditions favor one or the other (10). For instance, contribution from acetotrophic methanogens increases when the temperature decreases. Soil salinity also seems to be a relevant factor in methanogenesis, since hydrogenotrophy is prevalent in marine sediments, and acetotrophy dominates methane production in lake sediments (11), although this trend must not be generalized (6). Despite this, CH_4 flux into the atmosphere is not solely influenced by methanogenic Archaea, but also by methane-oxidizing microorganisms, known as methanotrophs, which carry out the opposite process, but unlike methanogens, can metabolize CH_4 aerobically (12,13).

Despite being a key player in the greenhouse effect, CH_4 plays a much bigger role in the carbon cycle. After being released into the atmosphere, methane molecules undergo oxidation, which results in the formation of CO_2. The latter eventually re-enters the biosphere through photosynthesis, thanks to plants and algae, which produce carbohydrates that may be consumed by other organisms, or be deposited in soils in terrestrial ecosystems, such as wetlands (6). In the peats is where methanogens

transform these carbon-based compounds into methane in one of the two aforementioned anaerobic metabolic pathways, where, eventually, the cycle starts again, via diffusion through soil, ebullition in water or transport from the rhizosphere through aerenchyma of vascular plants. In the former two, there is high probability that methane is oxidized either anaerobically or aerobically by Bacteria and Archaea, hence balancing the net flux and creating carbon sinks, instead of carbon sources. The importance of carbon sequestration by wetlands and other ecosystems cannot be overlooked, since it maintains the equilibrium between emission and consumption of methane, as well as carbon dioxide. Nonetheless, climate change an ecosystem destruction of páramos threaten their role as a carbon sink by releasing both of these gases into the atmosphere, in a positive feedback system that magnifies the greenhouse effect on the planet (14).

In the past, methane emissions have varied greatly as a consequence of climatic and geographic phenomena; in this regard, temperature seems to be the most influential factor in CH_4 production and release to the atmosphere, due to release of methane trapped in melting ice and permafrost (15). As with CO_2, atmospheric CH_4 has also peaked after the industrial revolution, thus the increased concentration is attributed to human activities (1). During the Quaternary, particularly during the last million years, methane has had a shifting behavior with the most recent low during the Last Glacial Maximum 22 ky BP (kiloyears Before Present means thousands of years before AD 1950) (16). This trend is repeated during the Ice Ages of the Pleistocene, where increases in global methane concentration match interstadial phases, namely the warmer periods in recent geological history (17,18). In most recent times during the Holocene, although less variable than during the Pleistocene, CH_4 has had three key changes, at the beginning of the period 11.7 ky BP, between 8 and 9 ky BP, and in the last 300 years. The first one corresponds to a decrease during the Younger Dryas, followed by an abrupt rise before the Preboreal stage (10.3 ky BP) (19). The second one follows the previous one by a decline in atmospheric concentration, whereas the third one, as mentioned before, is the result of anthropogenic activities (20,21). Some studies, by means of climatic modelling and $\delta^{13}C$ isotopic signature, suggest that steep increases in atmospheric methane in the past 5 ky are due to a higher contribution from tropical wetlands and rice cultivation as a consequence of human demographic expansion and the spread of agriculture (22,23). Nonetheless, rapid shifts in methane, rather than being the driver of climate changes, have been a consequence of other factors, primarily Earth orbital fluctuations, most notably precession (16).

As stated early, tropical wetlands are understudied ecosystems concerning their role in climate change, specifically regarding their contribution to global warming through gas emission (24). These biomes comprise mainly mangroves and marshes along coasts, and peatlands distributed along a wide altitudinal range. The latter represents a special case as a result of the high levels of carbon deposited in its soils by plants (25,26); therefore, their contribution to methane emissions is more relevant (27). In the Neotropics, a unique type of peatland, known as páramo is located at the peak of the Andes Cordillera above 3000 m. This type of wetland ecosystem has been labeled as a biodiversity hotspot (28), although, it is currently threatened by mining and agricultural activities, as well as rising temperatures and change in rainfall regimes, inherent consequences of climate change dynamics (24). Just as other tropical wetlands, páramos overall ecology is yet to be explored, so as to determine their historical and future contribution to the current climatic phenomena (29).

In consequence of the above, shifting environmental conditions have had a direct impact on the carbon cycling of páramos for the last 12.000 years, hence in the overall methane flux. In order to

assess changes in time of CH_4-related activity, several geochemical signals are necessary as indicators of environmental variability; for instance, the concentration of certain metals in sediments point out water availability or reduction conditions, which are key factors in methanogen activity. Besides this, due to the impossibility of culturing Archaea under lab conditions, molecular characterization has been the main method in meta-population studies (30–32). Environmental DNA (eDNA) has been the focus of several (paleo)ecological reconstructions, not only of past fauna and flora, but also of microbe communities from environmental samples such as permafrost and lake sediments (33,34). In the present study, we aim to reconstruct methanogen communities from a páramo peatbog located in the Northern Andes of Colombia. To accomplish this goal, we made use of eDNA methodologies, specifically metabarcoding of the V3 region of the 16S rRNA prokaryotic genome. Having determined the community diversity, we were able to compare these results with other approaches, such as X-Ray Fluorescence, $\delta^{13}C$ of the sediments. All these procedures were within the framework of a Bayesian Age-Depth model, calculated with sediment samples from the core and resulted with the core covering most of the Holocene (~8.900 years).

Methods

Site Description

The Matarredonda Ecological Park (4'34° N, 74'00°) at 3,300 – 3,500 m, is located in the Eastern Cordillera of Colombia, 18 km to the East of Bogotá in the Department of Cundinamarca. This park contains several patches of páramo such as El Verjón and Cruz Verde. As part of a larger system of mountains in the capital of Colombia, known as the Eastern Hills (*Cerros Orientales* in Spanish), these ecosystems are marked by a high variance in the temperature on a daily scale, and a relatively constant precipitation regime throughout the year. Although precipitation in Northern South America is largely controlled by the Intertropical Convergence Zone, water availability is distinct in both sides of the Cordillera, particularly in the Eastern Cordillera, where the rain regime of the East side is controlled by orographic lift caused by the trade winds, which causes the West side to be drier and to have a bimodal annual cycle (35). For instance, as shown in **Figure 1**, the average annual precipitation in Bogota (**D**) between 1981 and 2010 was 841.2 mm, whereas Choachi (**E**), the closest town to Matarredonda, had an annual average of 1234.7 mm in the same period.
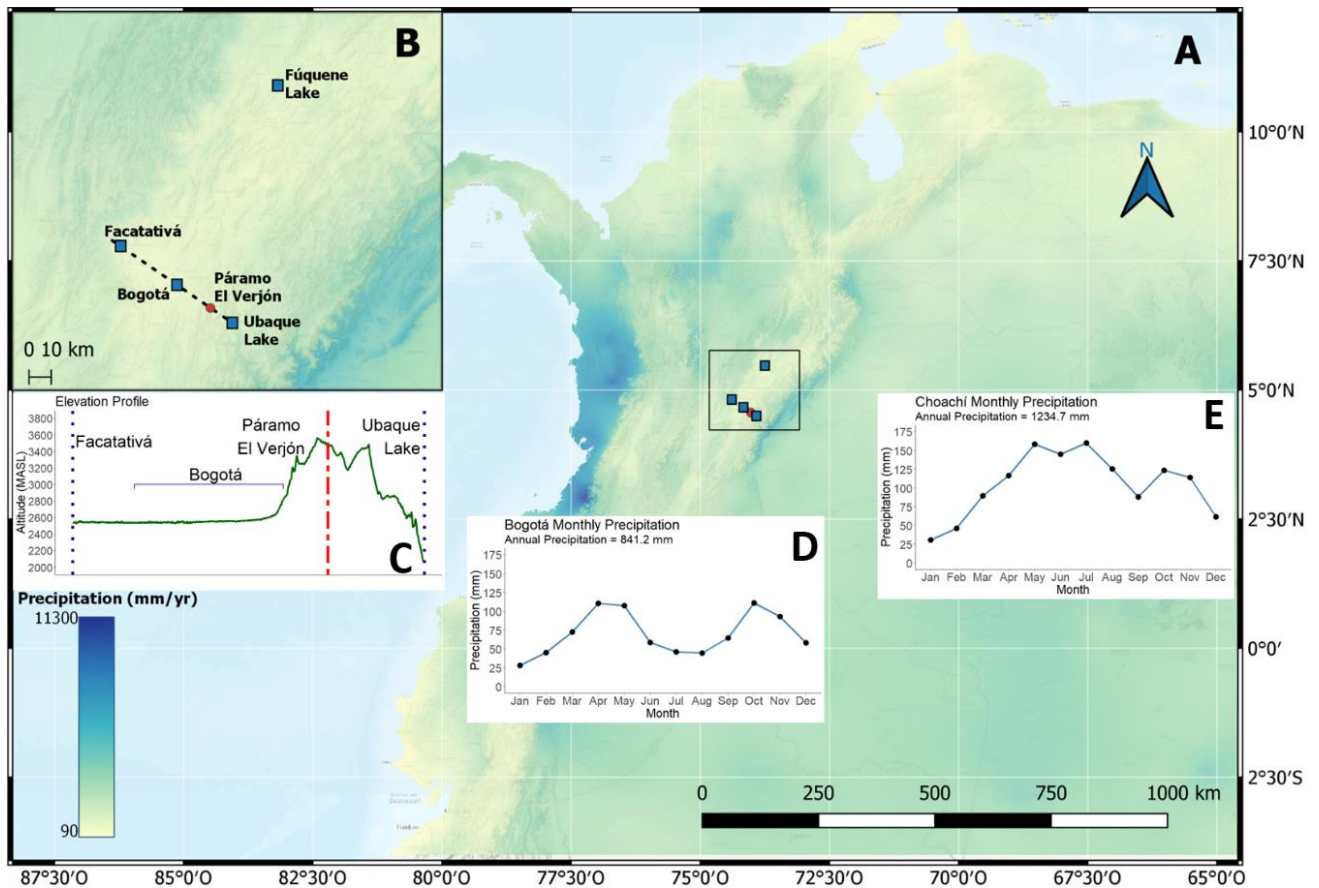
Figure 1. A: Annual precipitation in Colombia and the Andes Cordillera. B: Annual Precipitation in the region surrounding Bogota and Páramo El Verjon. C: Elevation profile from Facatativa to Ubaque Lake, passing by Bogota and Páramo El Verjon. D: Average annual precipitation cycle for Bogota from 1981 to 2010. E: Average annual precipitation cycle for Choachi from 1981 to 2010 (the closest town to Matarredonda Ecological Park).

Sediment Sampling and Description

A 1.5 m sediment core was raised using a Russian corer in 50-cm segments. The core, named VERJON-1, was described in-field regarding color changes and marked stratigraphical differences among layers of sediment. Subsequently, the core was sealed with plastic film and transported to the Laboratory of Tropical Palynology and Paleoecology, where it was kept in a freezer at 4 °C. After that, the core was taken to a different room where no molecular assays had been performed before, where sub-sampling for every analysis took place. About 1 cm of surface sediment was removed before DNA subsampling in order to minimize risk of contamination. For the organic matter, X-Ray Fluorescence (XRF) and isotope content, sub-sampling was done every 1 cm, for a total of 150 subsamples.

Chronology and Age Model

Chronology of VERJON-1 was established based on four bulk AMS C14 dates from depths 4, 54, 82, 134 cm. These samples were dried for three days at 40 °C. The first two samples were dated at DirectAMS, Seattle, USA; while the last two were dated at ETH Zurich, Switzerland. Based on the

AMS measuring of the four samples, the age model was stablished with the Bacon software, distributed as a R package named *rbacon* v2.3.9.1. This set of tools uses Bayesian Statistics to perform an age-depth model using radiocarbon dates (36). The calibration curve used for the calibrated dates is IntCal 13 (37,38), which is used for Northern Hemisphere terrestrial samples. In addition, in the process it was assumed that the top of the core (0 cm) is from 2018, for which the Northern Hemisphere Zone 2 (NH Zone 2) calibration curve was used, in order to correct post-nuclear bombs ages. This consideration means that in the calibration process, negative ages are possible, which correspond to post-1950 years (39).

Organic Matter Content

Loss-on-ignition (LOI) was carried every 1 cm in order to estimate the water content and organic matter content in the sediments. For this purpose, between 1 and 2 grams of sediment sample were weighed in a crucible and placed in a furnace at 105 °C overnight. After this step, crucibles were re-weighed to find water content. Finally, the same crucibles were placed in the furnace at 550 °C and re-weighed to estimate organic matter content (40).

Geochemical Elements: X-Ray Fluorescence (XRF)

Geochemical elemental composition was analyzed every cm throughout VERJON-1, from which 2 g were dried for 4 days at 50 °C in a furnace and placed in plastic bags. The detection of geochemical elements by X-Ray Fluorescence (XRF) was performed using a XMET 7500 handheld portable analyzer at the Geosciences Laboratory of Universidad de los Andes. This tool permits the detection of over 30 elements, mostly metals, such as titanium, potassium and manganese, which are a valuable paleoecological record of past environmental conditions. These elements present are raw count, therefore a log normalization is used, both in single and ratio index for further analysis (41,42). In addition, the proportions of these elements, such as sulfur and titanium result in complementary information (42). The dried samples were powdered using a mortar and placed on the detection unit of the pistol for 1 minute, in duplicate per each sample.

δ^{13}C Isotopic Signature

During the conversion of CO_2 into methane under anoxic conditions in e.g. peatbogs or lake sediments, the fractionation processes of fermentative production of acetate results in a clear enrichment of Carbon-13 isotopes (δ^{13}C). Therefore, by analyzing the δ^{13}C signature of the organic fraction of sediments, it is possible to track back the methanogenic activity along the core in an independent way, with a much higher resolution, and compare it to the molecular approach at specific intervals (43). For δ^{13}C measure, between 0.9 mg and 1.1 mg of dried sediment was weighed in a microbalance and packed in a tin capsule and placed in 96-wells plates, for every section of VERJON-1 for posterior analysis at the Environmental Stable Isotope Laboratory of the University of Leicester, United Kingdom.

eDNA Analysis

Due to high sensitivity to contamination, eDNA procedures must be carried out under strict conditions, so as to minimize the risk of detecting false positives that belong to external sources of DNA. As stated above, samples were kept in a refrigerator at 4 °C before sub-sampling; the latter process was done by using sterile scalpel and forceps that were previously treated with UV light for

one hour, as well as wearing nitrile gloves and lab coats (44) to recover sediment from the inner part of the core. These sub-samples were collected from the core in duplicate every 10 cm with a sterile syringe, and subsequently placed in a freezer at -20 °C for DNA conservation, until molecular assays started (45).

As detailed in the previously, special considerations must be met when working with highly degraded DNA (44); therefore, all the extraction protocols and pre-PCR procedures were performed in the ancient DNA (aDNA) laboratory of Universidad de los Andes. The protocol used for DNA isolation from soil is Qiagen DNeasy Powermax Soil Kit (formerly known as MoBio Powermax Soil DNA Isolation Kit) (Germany), following the manufacturer's manual (32,46,47). A negative control was included with every replicate batch, thus there were two different negative controls for the extraction stage. In total, there we 17 extractions and their respective replicates. Concentrations and purity were quantified using NanoDrop.

Because of the environmental conditions of the deposition site, large fragments of eDNA are unlikely to be found, hence a complete amplification of the 16S rRNA region, which comprises more than 1,500 bp, is unrealizable. Consequently, a shorter fragment within this region must be selected, so as to be adequately diverse to be used as a barcode for Archaea species (48); previous studies have reported primers for the amplification of one or some of the nine hypervariable regions contained in 16S (49); however, several of these amplicons fall out of the range of eDNA, with sizes larger than 200 bp. A recent study (50) determined that the V3 region is a formidable target for eDNA recovery due to its length and variability, by using the U341F/534R set of primers, whose product size is 150-194 bp, shown in **Table 1**; these primers were modified with a 5' tag in each one, according to specifications from the sequencing service were this step was performed (50,51). Since doing all molecular steps until sequencing was not possible, five sub-samples were selected according to XRF and Loss-on-ignition results for amplification; these samples correspond to depths 10, 50, 80, 100 and 120 cm. In total there were three PCR reactions per extraction replicate, for a total of six amplification reactions. Each one of these reactions included the five selected samples, the extraction negative control, plus a negative control for the PCR and a positive one, which was DNA of a non-methanogenic Archaea, *Haloferax chudinovii* (kindly donated by the USBA laboratory at Universidad Javeriana de Bogotá). The final count of individual tubes was 48. The PCRs were performed using the AmpliTaq Gold® 360 DNA Polymerase and Master Mix (Thermo Fisher Scientific, MA, USA), following manufacturer's recommendations with total volume of 25 μl. Regarding reactant concentrations, the PCR conditions set in a thermocycler were: an initial activation process of 10 minutes at 95 °C, continued by 35 cycles of 30 seconds at 98 °C (denaturation), 30 seconds at 68 °C (annealing) and 60 seconds at 72° C (elongation), followed by a 7-minute extension at 72 °C (50).

Table 1. Sequence of primers and tags added to the 5' end of each one for the amplification of V3.

PRIMER NAME	TAG SEQUENCE	PRIMER SEQUENCE
U341F	ACACTGACGACATGGTTCTACA	CCTACGGGRSGCAGCAG
534R	TACGGTAGCAGAGACTTGGTCT	GWATTACCGCGGCKGCTG

Following the amplification step, each one of the six positive controls from the PCR were pooled equimolarly in one. Both amplicon purification and sequencing were done at the Institute for Genomic Sciences at University of Maryland, USA, in an iSeq 150 system with paired end reads.

The sequences obtained in the previous step were processed using QIIME2 v2019.7 (52), which is a platform specialized in microbiome analysis that allows the filtering, cleaning and pairing of the sequences, as well as the taxonomic assignment of OTUs (53). The sequences were demultiplexed according to a unique sample and replicate ID. Subsequently, low quality reads were removed using the DADA2 plugin. Since six PCRs were run for every sample, the reads were grouped by the sample depth they belonged to and averaged for the subsequent steps.

In order to annotate the taxonomy of each sample read, a custom database was constructed for the V3 region from the latest SILVA 16S reference dataset (54) using the untagged primer sequences. This was trained according to taxonomy at the species level using the Naive-Bayes Multinominal algorithm from the feature-classifier plugin, which uses sci-kit learn v0.21.2.

Finally, after taxonomy assignment, non-significant taxa were removed (Eukaryotes, Bacteria and non-methanogenic Archaea) and alfa biodiversity was estimated from the samples using Shannon's diversity index and Beta diversity was calculated with a Bray-Curtis dissimilarity matrix (33,55).

Results

Sediment Description

The description of visible characteristics of VERJON-1 was done in field, where two main zones were detected based on the color of the sediments, which indicates organic matter and water content. Above 125 cm the sediment was dark with different layers further emphasized in **Figure 2**. Below 130, a more mineral nature was evident with a yellowish color; nonetheless, there is a transition zone from organic to mineral dominance between 126 and 133 cm. As a result of this, the latter section was selected for carbon dating, since this element was not abundant in deeper sections.
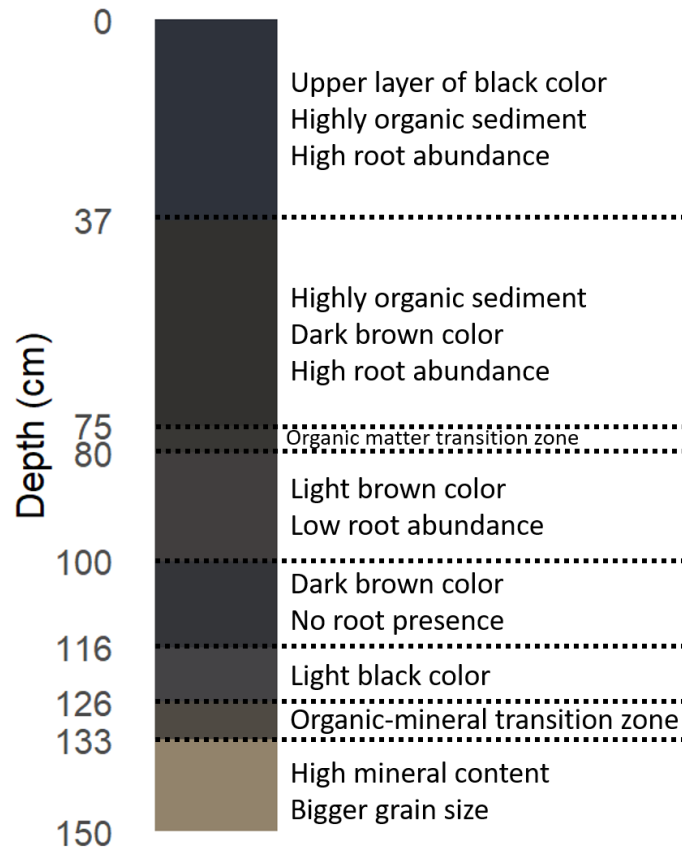
Figure 2. VERJON-1 core stratigraphy and sediment description in-field.

Chronology and Age model

The Bayesian Age-Depth Model was calculated using sections of organic nature along VERJON-1 core, hence the reason why the bottom was not dated (**Table 2**). Nonetheless, since the curve for the two deepest dated samples is linear (**Figure 3**), the estimated ages for the last 15 cm were calculated (**Supplementary Table 1**). It is worth noting that the section that corresponds to 0 cm was assumed to be 2018 in the calibration process, meaning post-1950. However, no other age was estimated to be later than nuclear bomb years.

Table 2. C^{14} Ages, errors and calibrated errors for four sections of VERJON-1.

DEPTH (CM)	C^{14} AGE BP	ERROR (±1σ)	CALIBRATED AGE (MEDIAN)	CALIBRATED AGE (MIN)	CALIBRATED AGE (MAX)	LABORATORY
4	214	35	178	65	344	DirectAMS
54	4454	34	4764	4376	4976	DirectAMS
82	5459	23	6217	6096	6309	ETH Zurich
134	8248	33	8922	8427	9448	ETH Zurich

Figure 3. *Age-Depth Model for VERJON-1 using the Intcal13 calibration curve and NH Zone 2 curve for post-bomb ages. Median ages for each depth are shown in red; maximum and minimun estimated ages are depicted in blue.*

Organic Matter (OM) Content

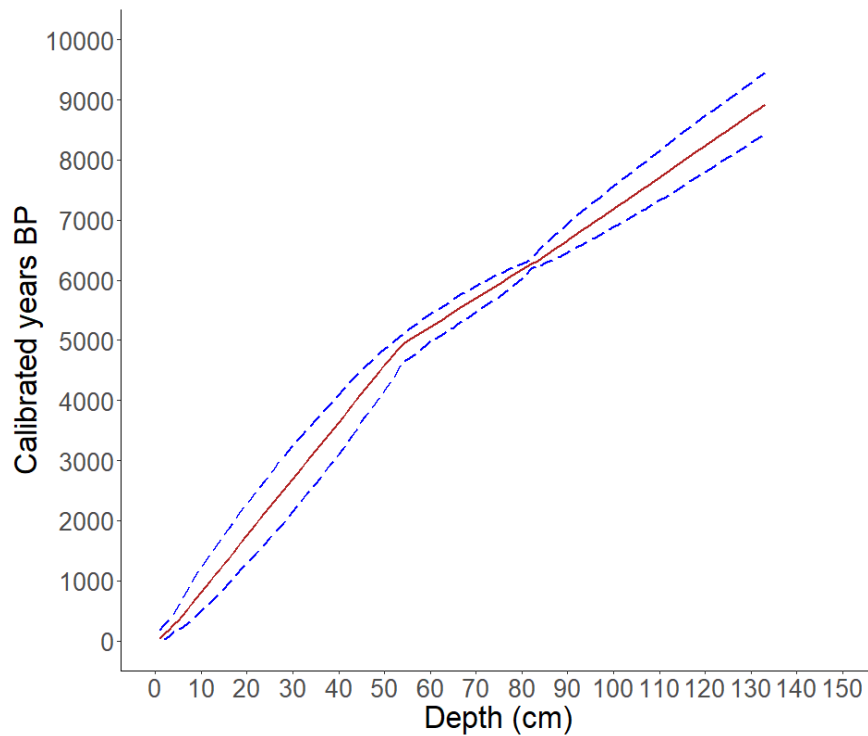In the deepest part of the section between 120 and the bottom, organic matter measured as a LOI percentage, was lowest varying 10-30%. Contrastingly, in the above this range estimated organic matter varied between 30% and 70% of its original weight. Despite this high carbon content, between 66 and 87 cm, there is a visible drop in organic matter content. These changes in organic matter are also visible in Figure 3, where the mineral color of mineral part signals less carbon content, whereas the rest of the core, although highly variable, LOI values are generally higher.

Geochemical Elements: X-Ray-Fluorescence (XRF) Analysis

XRF enabled the measurement of relative counts of several elements, such as Aluminum (Al), Silicon (Si), Phosphorus (P), Sulfur (S), Chlorine (Cl), Potassium (K), Calcium (Ca), Titanium (Ti), Vanadium (V), Chromium (Cr), Manganese (Mn), Iron (Fe), Cobalt (Co), Nickel (Ni), Copper (Cu), Zinc (Zn), Rubidium (Rb), Strontium (Sr), Zirconium (Zr), Niobium (Nb), Molybdenum (Mo), Cadmium (Cd), Tin (Sn), Antimony (Sb), Barium (Ba), Tantalum (Ta), Mercury (Hg), Tungsten (W), Lead (Pb) and Uranium (U). Despite finding 30 elements, some of them, given the characteristics of the sampling site, are unlikely to be found, therefore, they were assumed as errors of the measurement unit. This was further confirmed by their low frequency (< 25 measurements) in the data in the following elements: Cr, Co, Cu, Cd, Sn, Sb, Ta, W, Pb, U and Hg; in addition, most of them are not relevant for the current study, but are more significant when assessing mining and pollution in soils (56). Further, with the remaining elements, some ratios can be calculated which are relative indicators of several environmental processes through time; such as weathering, organic matter input and rainfall changes (42).

δ^{13}C Isotopic Signature

The isotopic curve for the VERJON-1 core presents a homogeneous behavior, with values ranging from -25 to -23 ppm generally. Nonetheless, it is worth highlighting two drops at 20 and 120 cm, and subtle increases between 70 and 100 cm. In addition, further work needs to be carried out, in order to complete and replicate the zones where this index is missing.

Since several measurements were made to characterize the sediments at a chemical level, a correlation matrix was performed, in order to assess the relationship between variables using a Pearson correlation, as shown in **Figure 4**.
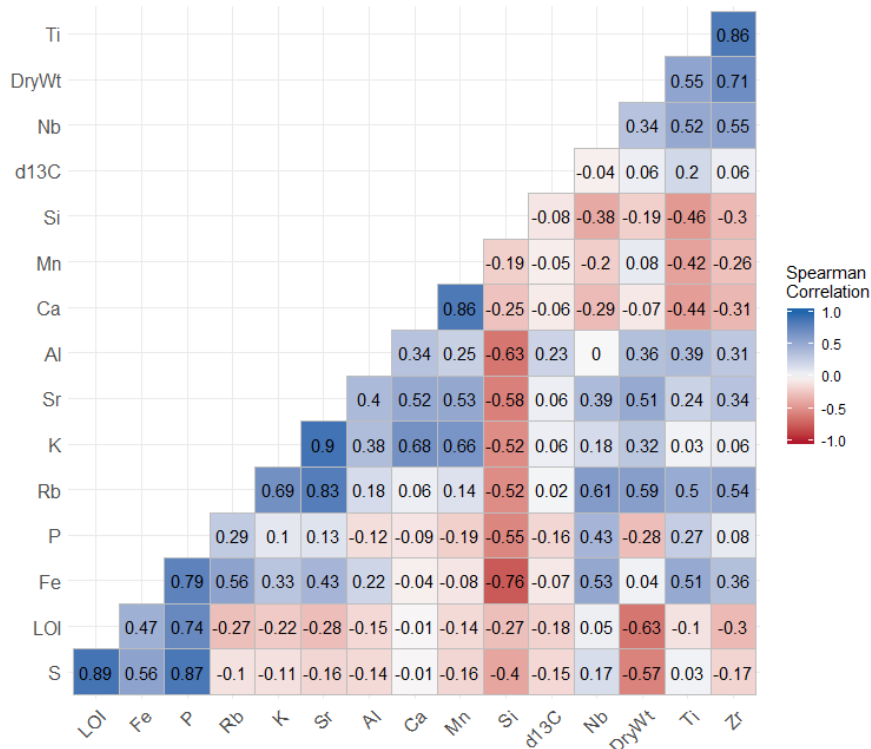
Figure 2. Spearman correlation matrix among the distinct measurements of the present study.

There are certain correlations, both positive and negative, that were expected; for example, LOI and dry weight show distinct yet related behavior since organic sediments tend to be wetter, but more mineral sections lack humidity, since water is not available in the deepest part of the core.

eDNA Analysis

With the advancement in molecular biology in the last 25 years, both extant and extinct groups of species can be profiled with the use of environmental DNA (eDNA) (57). DNA has a rapid decay rate and its preservation depends heavily on certain environmental conditions of the deposition site, notably, temperature and water (58). As a result of this, eDNA is unlikely to be extracted in large sizes, thus stringent handling precautions of the samples must be taken, in order to avoid

contamination with modern DNA (44). The latter is of special significance for profiling of prokaryotic communities/species because of the abundance of potential sources of contamination in every step from sampling in field to laboratory work (59). In páramos, water is present year-round, and it has been reported that it facilitates DNA degradation; therefore, DNA is likely to be found in short fragments, such as in ancient environmental DNA studies (60). Despite this, barcoding has been applied on studies both of past and present microbial communities (34,61) but, owing to fragmentation, primers for the whole 16S rRNA region cannot be utilized for this purpose (62); consequently, one of the nine hypervariable regions within 16S must be targeted. Primers for the V3 region have been reported for aDNA of Bacteria, because the fragment size (~1600 bp) falls within the range of expected length to be found (63,64). Although not tested in Archaea species, 16S-based metabarcoding has enabled the identification of Bacteria and Archaea species in other environmental surveys, hence, identification of methanogen species using V3 region is set to yield promising results (34).

In general, according to the Nanodrop measurements for both replicates, DNA concentration decreases with depth, as expected; nonetheless, samples from 20 and 40 cm had the highest nucleic acid content of all the sediment core, as shown in **Figure 5**.
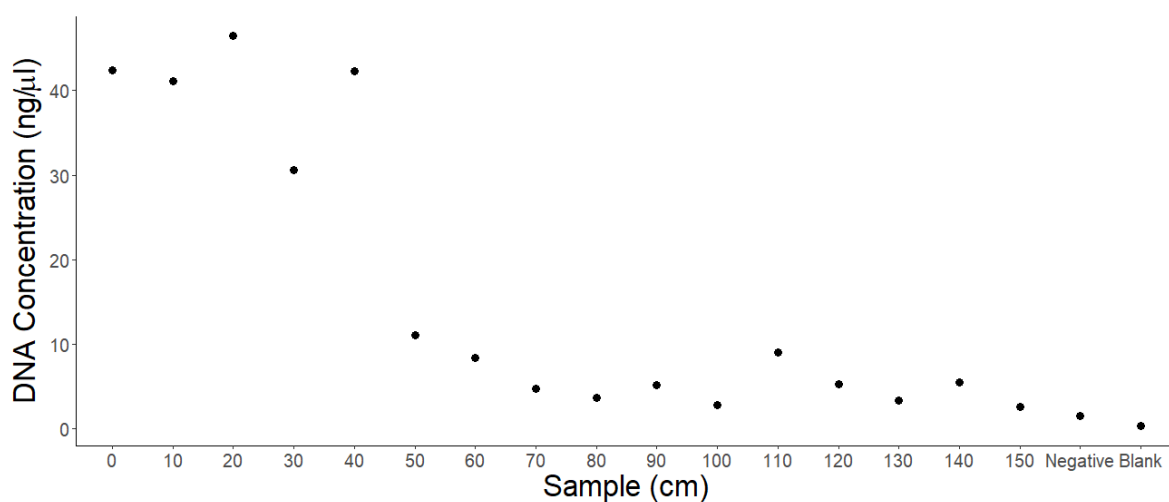
Figure 3. Average DNA concentration across VERJON-1 core for the two replicates, plus the extraction negative control and the Nanodrop blank.

Due to the variability in DNA concentration and sediment characteristics, amplification could not be performed on all the extractions. Instead, as stated in the methods, five samples were selected for this analysis. However, a standardization of this process was performed using 7 ng of DNA for each sample in every PCR reaction. The corresponding volume was used in each one of the three PCR replicates for the two extraction replicates, for a total of six reactions per sediment section.

Despite having assessed the performance of each PCR reaction and its corresponding controls with agarose gels for each batch of replicates as shown in **Figure 6**, the sequencing process, in spite of producing 1.2 Gb of information represented by 7.688.000 reads, did not yield high-quality sequences, from which a bioinformatic analysis could be performed. Double index barcodes were assigned to every sample replicate, however, an identification of the reads according to sample

was not possible due to the high frequency of undefined bases (e.g. high abundance of N bases). In addition, the sequence belonging to *Haloferax chudinovii*, the PCR positive control, could not be found among the reads, thus suggesting a low quality of the barcode assembly and posterior sequencing run.
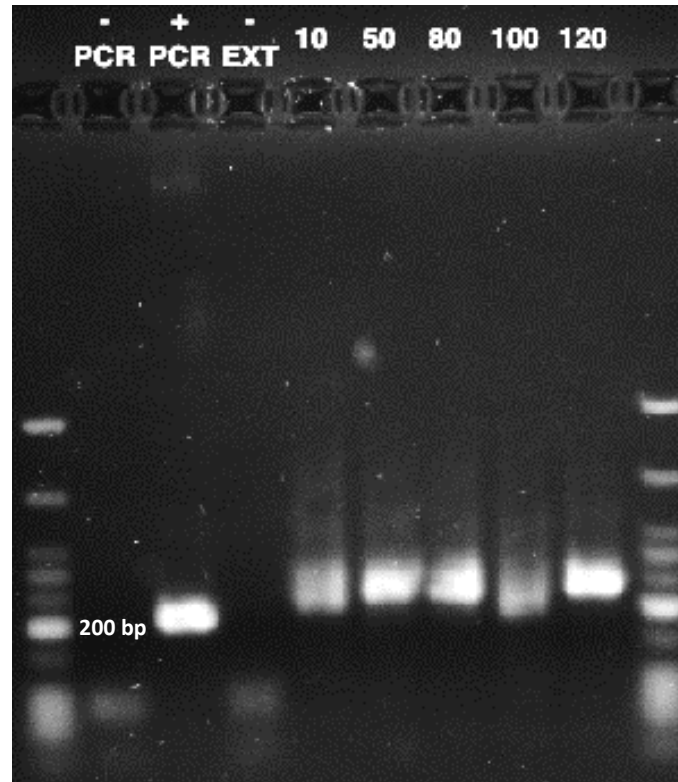
Figure 6. Agarose Gel of PCR results for the V3 region of 16S. The first and last wells are the molecular ladder, where the 200 bp band is indicated; -PCR is the negative control; +PCR is the positive control using Haloferax chudinovii DNA; -EXT is the amplification of the negative control of the extraction process; 10, 50, 80 and 120 are the depths of sediment samples for which the amplification process was successful.

Discussion

First and foremost, it is worth noting that VERJON-1 is the first paleoecological record from a páramo of the Eastern Cordillera in Northern South America, that has been studied in terms of climatic history and carbon cycling from a geochemical perspective. In addition, it represents one of the most complete records given the timespan it covers (~8920 yr), since previous studies have shown deeper cores that cover a shorter period of the Holocene; for instance, Van der Hammen work on this Cordillera, albeit focused on plant communities changes via palynological records, included sediment cores twice as long, but the time span was similar to that covered by VERJON-1 (65). This means that sediment accumulation rate has been generally higher at Páramo El Verjon than in most other páramos of Colombia. Nonetheless, this deposition velocity has fluctuated over the last 9.000 years, according to VERJON-1 as shown in **Figure 7A**; during early Holocene up until 5.000 years BP accumulation rate has oscillated around 0.05 cm/year. Meanwhile, between 5.000 and 200 years BP, this index dropped half. However, according to the Bayesian model, in the last 200 years a considerable rise is visible, which corresponds to the period were human activity has concentrated the most in the Colombian Andean region, roughly pinpointing the start of the

Anthropocene. This behavior is consistent with reported studies of lakes from the Eastern Cordillera, where carbon deposited at a faster rate during the Early Holocene, but accumulation slowed in the most recent centuries (65).

Figure 7. *Organic geochemical indexes compared to the stratigraphic column of VERJON-1, adjusted for calibrated ages. A: Sediment accumulation rate in cm/years. B: Percentage of water content. C: Loss-on-ignition (LOI) as a measure of carbon content. D: $\delta^{13}C$ in ppm.*

Regarding the geochemical signal for methanogenesis, it has been consistently shown that anoxic environments are a requirement for Archaea species to produce CH_4, via anaerobic metabolism. Lack of oxygen in soil is reached when water availability is high, since it restricts the gas from flowing through the peat in wetlands. Despite high water content (**Figure 7B**) and LOI (**Figure 7C**) percentages indicating high water table level and high organic carbon, respectively, methane activity is not evident from $\delta^{13}C$ (**Figure 7D**). This variability is low compared to other wetlands (66); very negative values in this measurement (~-60 ppm) suggest higher overall methane activity, both production and consumption by soil microorganisms. Two negative zones are evident, although further work is necessary in order to assess the change in the isotopic signature of VERJON-1, concerning methane activity. Notwithstanding these findings, $\delta^{13}C$ in soils has been shown to correlate to plant composition, particularly to carbon fixation mechanisms in past vegetation; C3 plants are dominant in sediments with low $\delta^{13}C$, while C4 metabolism prevails in high $\delta^{13}C$ sediments (67). This relationship, although not directly related to CH_4, is an indicator of hydrological cycles in time, meaning drier conditions when C4 plants are present, and wetter conditions when vegetation is dominated by C3-like vegetation. When compared both LOI and $\delta^{13}C$ curves, the peaks in the latter roughly match the lowest levels of the former in the organic

matrix of the core, possibly meaning a decrease in methanogenesis, between 6.500 and 5.500 years BP, as a result of low water column levels.

Unlike the previous geochemical proxies, inorganic elements show higher variability throughout time, and some show similar trends as seen in **Figure 8**. One of the most striking findings is that peaks in K (**Figure 8A**), which has been reported as an indicator of drier conditions, correlate with those of Mn (**Figure 8B**), which signals oxygenated bottom water, hence lower water column. Both columns have high values in the same interval as $\delta^{13}C$ and LOI, thus supporting the hypothesis of a lack of rainfall at the end of early Holocene that could rise water table and anoxic conditions in páramos sediments. In addition, Ti (**Figure 8C**) has been largely used as a proxy for rainfall (68,69), and although it does not match its lowest points, it has a significant decrease around 6.500-5.500 years BP. Some ratios of the XRF reads also provide valuable information about past environmental conditions; for instance, in previous works in South America (70), S/Ti (**Figure 8D**) has been correlated with organic matter content in sediments, which is also the case with VERJON-1.
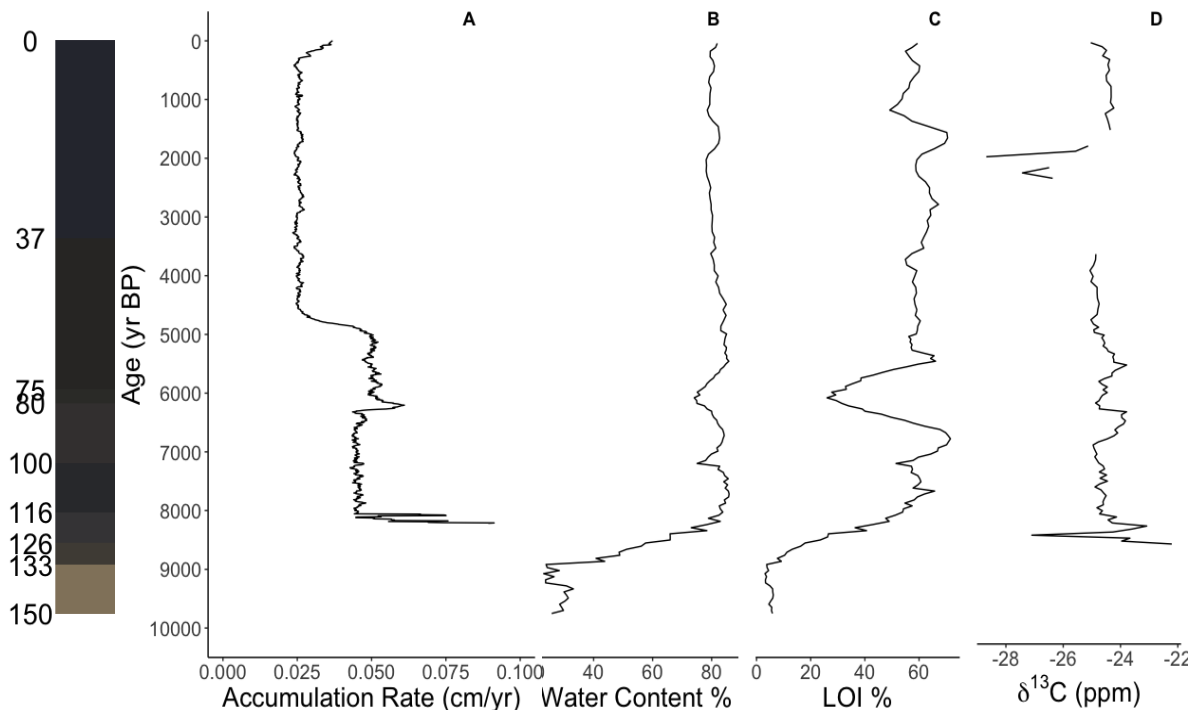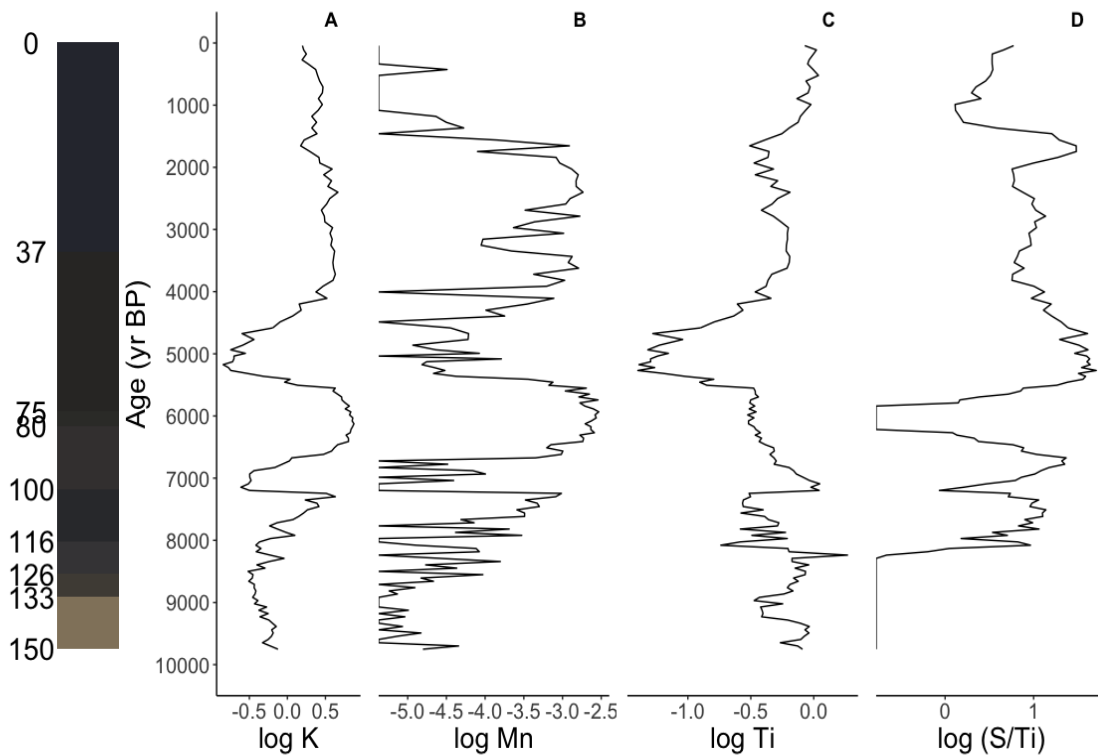

Figure 8. Log-normalized Inorganic geochemical indexes compared to the stratigraphic column of VERJON-1, adjusted for calibrated ages. **A:** Potassium (K). **B:** Manganese (Mn). **C:** Titanium (Ti). **D:** Ratio of Sulfur and Titanium (S/Ti).

At a regional scale, hydrological cycles in Northern South America have varied greatly in the last 10.000 years, meaning that water availability has changed over time in most ecosystems. In páramos, this suggests that methane production activity could be affected by changes in the local rainfall regimes. For instance, the Cariaco basin in Northern Venezuela has a rich paleoecological record of the Neotropics ocean climate, which ultimately plays a key role on precipitation on the

continent. Haug et al. (2011) (71) found evidence for a change in the latitudinal position of the Intertropical Convergence Zone (ITCZ) in the form of Titanium concentration during the early Holocene, more precisely further north from the equator, in a period also known as the Holocene Thermal Maximum. What this means is that both temperature and precipitation increased. Whereas in the second half of the Holocene both variables decreased significantly, meaning drier conditions. On the other hand, records of grain size, specially sand, from El Junco lake in the Galápagos islands show the variability of the El Niño Southern Oscillation (ENSO) during most of the Holocene; in consistence with the Cariaco results, Conroy et al. (2008) (72) show that ENSO has strengthened in the latter millennia, meanwhile during early to middle Holocene ENSO had a milder effect on the climate of South America. These findings suggest that at two periods, more precisely between 5.100-4.100 and 7.100-6.8000 years BP, enhanced ENSO frequency likely caused more severe droughts at the Cordillera Oriental de Colomba . Considering the above, methanogenesis in páramos is assumed to have decreased in those two periods, which, along the Cariaco records suggest that regional climate phenomena such as ENSO and ITCZ latitudinal shift have a direct effect on the hydrological cycle of páramos, hence, on methane production in the peats of these high-mountain wetlands. As seen in **Figure 9**, dry periods recorded in sand from El Junco Lake (**Figure 9A**) and those detected by Potassium (K) XRF signal in VERJON-1 (**Figure 9B**) match in periods where ENSO has been more intense in Northern South America, meaning drier periods for the Andes of Colombia. What this suggests is that in wetter periods with mild ENSO, water availability in páramos could favor methanogenic activity by creating anoxic conditions for Archaea, meanwhile, in dry periods the methane flux might have been unbalanced as a result of lower water availability and anoxia, as shown by the ratio of Fe/Mn (**Figure 9C**), which pinpoints reducing conditions, thus oxygen presence that could have limited metabolic anaerobic activity of methanogens, specially at 6.000 years BP, where the three proxies match.
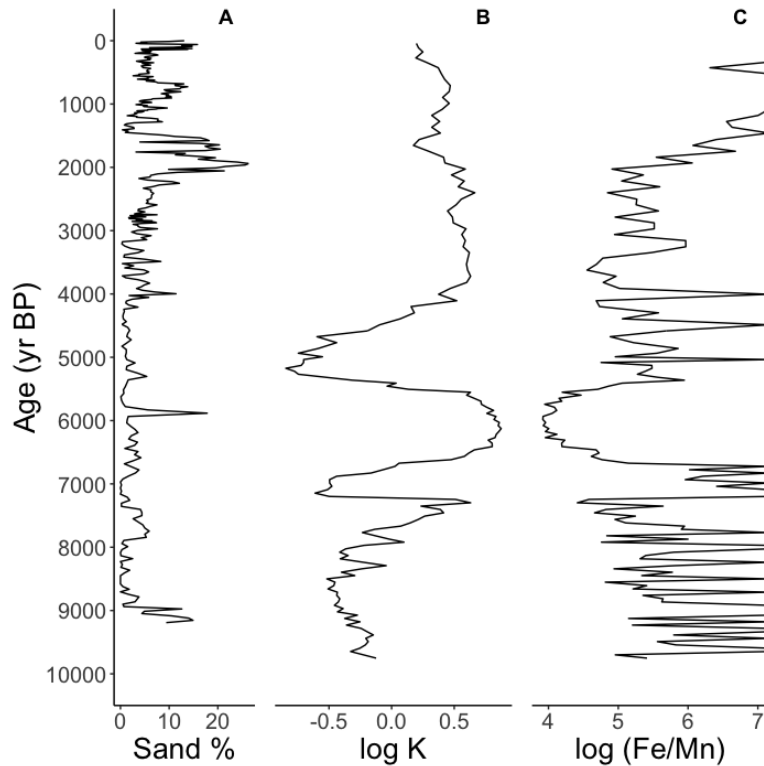
Figure 9. Geochemical proxies for climate variability of Northern South America during the Holocene. *A: Sand signature from El Junco lake of the Galápagos Island. B: Log-normalized Potassium (K) and C: ratio of Iron and Manganese (Fe/Mn) from VERJON-1.*

Finally, environmental DNA represents a unique way of assessing population diversity, but it also faces barriers when it comes to damages of nucleic acid structure by means of degradation caused by water and temperature, which are highly variable in páramos. Nonetheless, since microorganisms are ubiquitous in soil, particularly in organic matter-rich ones (73), DNA quantity was expected to be homogenous depth-wise; however, concentration decreased in deeper sections, which shows that micro-environmental conditions change drastically, which may favor DNA preservation. Moreover, lower organic-rich sections show no difference in DNA concentration compared to mineral sections. In contrast, the upper sections with high organic matter content contain the most DNA concentration in the core. This finding suggests that carbon availability is not a key player in microbial colonization of soil micro-habitats. Furthermore, most of eDNA found in sediment samples is expected to be from living organisms, with a littler proportion belonging to the ancient DNA (aDNA) realm, which by its nature, it is expected to be highly degraded and in low concentration. However, in order to separate eDNA from aDNA, a more comprehensive metagenomic approach is necessary, in which the latter can be detected by its low-frequency, deamination of cytosines and short length (74). In regard to methanogen community characterization, despite not being able to find significant sequences, wetlands have been reported to have a great taxonomic diversity, with most of the major orders present, aside from those groups that have only been found in hydrothermal vents in the ocean, such as Methanopyrales and Methanococcales, which follow the hydrogenotrophic pathway of methane production (75). Members of the hydrogenotrophic families Methanomicrobiaceae and Methanobacteriacea from the Methanobacteriales order, alongside the acetotrophic order

Methanosarcinales are commonly found in the wetlands of the Northern Hemisphere (76,77). Meanwhile, in the Neotropics, families within the latter order, such as Methanosaetaceae and Methanosarcinaceae, as well as several families from Methanobacteriales have been reported in Amazonian wetlands (73), Although no dominance has been stablished between methanogenic pathways for tropical or high-mountain wetlands (10,79).

References

1.   Lewis SL, Maslin MA. Defining the Anthropocene [Internet]. Vol. 519, Nature. Nature Publishing Group; 2015 [cited 2018 Apr 24]. p. 171–80. Available from: http://www.nature.com/articles/nature14258

2.   O'Connor FM, Boucher O, Gedney N, Jones CD, Folberth GA, Coppell R, et al. Possible role of wetlands, permafrost, and methane hydrates in the methane cycle under future climate change: A review. Rev Geophys [Internet]. 2010 Dec 23 [cited 2018 Apr 24];48(4):RG4005. Available from: http://doi.wiley.com/10.1029/2010RG000326

3.   Reay D ~Hrsg. . Methane and climate change Elektronische Ressource. 2010 [cited 2018 Apr 24];(December 2016):18–20. Available from: https://books.google.com/books?hl=es&lr=&id=0Xv6hA34G18C&oi=fnd&pg=PP2&dq=met hane+climate+change&ots=vrQSZokWpe&sig=Z6E0LUfw8d1UIB8nVpx8S6-oNhc

4.   Höglund-Isaksson L. Global anthropogenic methane emissions 2005–2030: technical mitigation potentials and costs. Atmos Chem Phys Atmos Chem Phys [Internet]. 2012 [cited 2018 Apr 24];12:9079–96. Available from: www.atmos-chem-phys.net/12/9079/2012/

5.   Fuller DQ, van Etten J, Manning K, Castillo C, Kingwell-Banham E, Weisskopf A, et al. The contribution of rice agriculture and livestock pastoralism to prehistoric methane levels. Ruddiman WF, Crucifix MC, Oldfield FA, editors. The Holocene [Internet]. 2011 Aug 1 [cited 2018 Apr 24];21(5):743–59. Available from: http://journals.sagepub.com/doi/10.1177/0959683611398052

6.   Blowes DW, Ptacek CJ, Jambor JL, Weisener CG, Paktunc D, Gould WD, et al. Treatise on Geochemistry [Internet]. Vol. 11, Treatise on Geochemistry: Second Edition. 2014 [cited 2018 Apr 4]. 131–190 p. Available from: https://www-sciencedirect-com.ezproxy.uniandes.edu.co:8443/science/referenceworks/9780080983004

7.   Mitsch WJ, Nahlik A, Wolski P, Bernal B, Zhang L, Ramberg L. Tropical wetlands: seasonal hydrologic pulsing, carbon sequestration, and methane emissions. Wetl Ecol Manag [Internet]. 2010 Oct 10 [cited 2018 Feb 11];18(5):573–86. Available from: http://link.springer.com/10.1007/s11273-009-9164-4

8.   Bridgham SD, Cadillo-Quiroz H, Keller JK, Zhuang Q. Methane emissions from wetlands: Biogeochemical, microbial, and modeling perspectives from local to global scales. Glob Chang Biol. 2013;19(5):1325–46.

9.   Laanbroek HJ. Methane emission from natural wetlands: Interplay between emergent macrophytes and soil microbial processes. A mini-review. Ann Bot. 2010;105(1):141–53.

10.   Galand PE, Fritze H, Conrad R, Yrjälä K. Pathways for methanogenesis and diversity of methanogenic archaea in three boreal peatland ecosystems. Appl Environ Microbiol [Internet]. 2005 Apr 1 [cited 2018 Apr 4];71(4):2195–8. Available from:

http://www.ncbi.nlm.nih.gov/pubmed/15812059

11. Hornibrook ERC, Longstaffe FJ, Fyfe WS. Spatial distribution of microbial methane production pathways in temperate zone wetland soils: Stable carbon and hydrogen isotope evidence. Geochim Cosmochim Acta. 1997;61(4):745–53.

12. Lee HJ, Jeong SE, Kim PJ, Madsen EL, Jeon CO. High resolution depth distribution of Bacteria, Archaea, methanotrophs, and methanogens in the bulk and rhizosphere soils of a flooded rice paddy. Front Microbiol [Internet]. 2015 Jun 25 [cited 2018 Apr 24];6:639. Available from: http://journal.frontiersin.org/Article/10.3389/fmicb.2015.00639/abstract

13. Segers R. Methane production and methane consumption--a review of processes underlying wetland methane fluxes [Review]. Biogeochem. 1998;41:23–51.

14. SERRANO-SILVA N, SARRIA-GUZMÁN Y, DENDOOVEN L, LUNA-GUIDO M. Methanogenesis and Methanotrophy in Soil: A Review. Pedosphere [Internet]. 2014 Jun 1 [cited 2020 Jan 21];24(3):291–307. Available from: https://www.sciencedirect.com/science/article/abs/pii/S1002016014600163

15. Hamdan LJ, Wickland KP. Methane emissions from oceans, coasts, and freshwater habitats: New perspectives and feedbacks on climate. Limnol Oceanogr. 2016;61:S3–12.

16. Singarayer JS, Valdes PJ, Friedlingstein P, Nelson S, Beerling DJ. Late Holocene methane rise caused by orbitally controlled increase in tropical sources. Nature [Internet]. 2011 [cited 2018 Apr 25];470(7332):82–6. Available from: https://www.nature.com/articles/nature09739

17. Bock M, Schmitt J, Beck J, Seth B, Chappellaz J, Fischer H. Glacial/interglacial wetland, biomass burning, and geologic methane emissions constrained by dual stable isotopic CH_4 ice core records. Proc Natl Acad Sci [Internet]. 2017;114(29):E5778–86. Available from: http://www.pnas.org/lookup/doi/10.1073/pnas.1613883114

18. Dean JF, Middelburg JJ, Röckmann T, Aerts R, Blauw LG, Egger M, et al. Methane feedbacks to the global climate system in a warmer world. Rev Geophys [Internet]. 2018;207–50. Available from: http://doi.wiley.com/10.1002/2017RG000559

19. Petrenko V V., Smith AM, Schaefer H, Riedel K, Brook E, Baggenstos D, et al. Minimal geological methane emissions during the Younger Dryas-Preboreal abrupt warming event. Nature [Internet]. 2017;548(7668):443–6. Available from: http://dx.doi.org/10.1038/nature23316

20. Etiope G, Milkov A V., Derbyshire E. Did geologic emissions of methane play any role in Quaternary climate change? Glob Planet Change. 2008;61(1–2):79–88.

21. Mayewski PA, Rohling EE, Stager JC, Karlén W, Maasch KA, Meeker LD, et al. Holocene climate variability. Quat Res. 2004;62(3):243–55.

22. Mitsch WJ, Nahlik A, Wolski P, Bernal B, Zhang L, Ramberg L. Tropical wetlands: seasonal hydrologic pulsing, carbon sequestration, and methane emissions. Wetl Ecol Manag [Internet]. 2010 Oct 10 [cited 2018 Apr 24];18(5):573–86. Available from: http://link.springer.com/10.1007/s11273-009-9164-4

23. Street-Perron FA. Ancient tropical methane. Nature. 1993;366(6454):411–2.

24. Buytaert W, Cuesta-Camacho F, Tobón C. Potential impacts of climate change on the environmental services of humid tropical alpine regions. Glob Ecol Biogeogr [Internet]. 2011 Jan 1 [cited 2018 Apr 26];20(1):19–33. Available from: http://doi.wiley.com/10.1111/j.1466-8238.2010.00585.x

25. Hribljan JA, Suárez E, Heckman KA, Lilleskov EA, Chimner RA. Peatland carbon stocks and accumulation rates in the Ecuadorian páramo. Wetl Ecol Manag. 2016;24(2):113–27.

26. Peña EJ, Sandoval H, Zuñiga O, Torres M. Estimates of carbon reservoirs in high-altitude wetlands in the colombian andes. J Agric Rural Dev Trop Subtrop [Internet]. 2009 [cited 2018 Apr 26];110(2):115–26. Available from: http://jarts.info/index.php/jarts/article/view/26

27. Teh YA, Diem T, Jones S, Huaraca Quispe LP, Baggs E, Morley N, et al. Methane and nitrous oxide fluxes across an elevation gradient in the tropical Peruvian Andes. Biogeosciences. 2014;11(8):2325–39.

28. Madriñán S, Cortés AJ, Richardson JE. Páramo is the world's fastest evolving and coolest biodiversity hotspot. Front Genet [Internet]. 2013 Oct 9 [cited 2018 Apr 26];4:192. Available from: http://journal.frontiersin.org/article/10.3389/fgene.2013.00192/abstract

29. Sánchez ME, Chimner RA, Hribljan JA, Lilleskov EA, Suárez E. Carbon dioxide and methane fluxes in grazed and undisturbed mountain peatlands in the Ecuadorian Andes. 2017 [cited 2018 Apr 26];19(20):1–18. Available from: http://www.mires-and-peat.net/,

30. Taylor GM, Mays SA, Huggett JF. Ancient DNA (aDNA) studies of man and microbes: general similarities, specific differences. Int J Osteoarchaeol [Internet]. 2010 Nov [cited 2018 Apr 25];20(6):747–51. Available from: http://doi.wiley.com/10.1002/oa.1077

31. Warinner C, Herbig A, Mann A, Fellows Yates JA, Weiß CL, Burbano HA, et al. A Robust Framework for Microbial Archaeology. Annu Rev Genomics Hum Genet [Internet]. 2017;18(1):annurev-genom-091416-035526. Available from: http://www.annualreviews.org/doi/10.1146/annurev-genom-091416-035526

32. Gorgé O, Bennett EA, Massilani D, Daligault J, Pruvost M, Geigl E-M, et al. Analysis of Ancient DNA in Microbial Ecology. In Humana Press, New York, NY; 2016 [cited 2018 Mar 19]. p. 289–315. Available from: http://link.springer.com/10.1007/978-1-4939-3369-3_17

33. Leonardi M, Librado P, Der Sarkissian C, Schubert M, Alfarhan AH, Alquraishi SA, et al. Evolutionary patterns and processes: Lessons from ancient DNA. Syst Biol. 2017;66(1):e1–29.

34. Ahmed E, Parducci L, Unneberg P, Ågren R, Schenk F, Rattray JE, et al. Archaeal community changes in Lateglacial lake sediments: Evidence from ancient DNA. Quat Sci Rev [Internet]. 2018 Feb 1 [cited 2018 Feb 11];181:19–29. Available from: https://www.sciencedirect.com/science/article/pii/S0277379117302858

35. Herzog S, … RM-… I for G, 2011 undefined. Climate change and biodiversity in the tropical Andes. museohn.unmsm.edu.pe [Internet]. [cited 2019 Oct 28]; Available from: http://museohn.unmsm.edu.pe/docs/pub_ictio/Josse 2011.pdf

36. Blaauw M, Christen J. Bacon manual–v2. 3.3. 2013 [cited 2019 Oct 28]; Available from: http://www.chrono.qub.ac.uk/blaauw/manualBacon_2.3.pdf

37. Reimer PJ, Bard E, Bayliss A, Beck JW, Blackwell PG, Ramsey CB, et al. IntCal13 and Marine13 Radiocarbon Age Calibration Curves 0–50,000 Years cal BP. Radiocarbon [Internet]. 2013 Feb 9 [cited 2019 Oct 28];55(4):1869–87. Available from: https://www.cambridge.org/core/product/identifier/S0033822200048864/type/journal_article

38. Niu M, Heaton TJ, Blackwell PG, Buck CE. The Bayesian Approach to Radiocarbon Calibration Curve Estimation: The IntCal13, Marine13, and SHCal13 Methodologies. Radiocarbon [Internet]. 2013 Feb 9 [cited 2019 Oct 28];55(4):1905–22. Available from: https://www.cambridge.org/core/product/identifier/S0033822200048888/type/journal_article

39. Hua Q, Barbetti M, Radiocarbon AR-, 2013 undefined. Atmospheric radiocarbon for the period 1950–2010. cambridge.org [Internet]. [cited 2019 Oct 28]; Available from: https://www.cambridge.org/core/journals/radiocarbon/article/atmospheric-radiocarbon-for-the-period-19502010/6BD120B674D0467B648CE1B8DF6428B8

40. Heiri O, Lotter AF, Lemcke G. Loss on ignition as a method for estimating organic and carbonate content in sediments: reproducibility and comparability of results. J Paleolimnol [Internet]. 2001 [cited 2018 Mar 19];25(1):101–10. Available from: http://link.springer.com/10.1023/A:1008119611481

41. Weltje G, Letters RT-E and PS, 2008 undefined. Calibration of XRF core scanners for quantitative geochemical logging of sediment cores: theory and application. Elsevier [Internet]. [cited 2019 Oct 28]; Available from: https://www.sciencedirect.com/science/article/pii/S0012821X08004974

42. Rothwell RG, Croudace I w. Micro-XRF Studies of Sediment Cores: A Perspective on Capability and Application in the Environmental Sciences. In 2015 [cited 2019 Oct 28]. p. 1–21. Available from: http://link.springer.com/10.1007/978-94-017-9849-5_1

43. Conrad R. Quantification of methanogenic pathways using stable carbon isotopic signatures: a review and a proposal. Org Geochem [Internet]. 2005 May 1 [cited 2018 Apr 4];36(5):739–52. Available from: https://www.sciencedirect.com/science/article/pii/S0146638004002566

44. Gilbert MTP, Bandelt HJ, Hofreiter M, Barnes I. Assessing ancient DNA studies. Trends Ecol Evol. 2005;20(10):541–4.

45. Bollongino R, Tresset A, Vigne JD. Environment and excavation: Pre-lab impacts on ancient DNA analyses. Comptes Rendus - Palevol. 2008;7(2–3):91–8.

46. Boessenkool S, Mcglynn G, Epp LS, Taylor D, Pimentel M, Gizaw A, et al. Use of ancient sedimentary DNA as a novel conservation tool for high-altitude tropical biodiversity. Conserv Biol. 2014;28(2):446–55.

47. Andersen K, Bird KL, Rasmussen M, Haile J, Breuning-Madsen H, Kjær KH, et al. Meta-barcoding of "dirt" DNA from soil reflects vertebrate biodiversity. Mol Ecol. 2012;21(8):1966–79.

48. Hajibabaei M, Smith MA, Janzen DH, Rodriguez JJ, Whitfield JB, Hebert PDN. A minimalist barcode can identify a specimen whose DNA is degraded. Mol Ecol Notes. 2006;6(4):959–

64.

49. Klindworth A, Pruesse E, Schweer T, Peplies J, Quast C, Horn M, et al. Evaluation of general 16S ribosomal RNA gene PCR primers for classical and next-generation sequencing-based diversity studies. Nucleic Acids Res [Internet]. 2013 Jan 7 [cited 2018 Mar 19];41(1):e1. Available from: http://www.ncbi.nlm.nih.gov/pubmed/22933715

50. Ziesemer KA, Mann AE, Sankaranarayanan K, Schroeder H, Ozga AT, Brandt BW, et al. Intrinsic challenges in ancient microbiome reconstruction using 16S rRNA gene amplification. Sci Rep. 2015;5:1–20.

51. Soergel DAW, Dey N, Knight R, Brenner SE. Selection of primers for optimal taxonomic classification of environmental 16S rRNA gene sequences. ISME J. 2012;6(7):1440–4.

52. Bolyen E, Rideout J, Dillon M, … NB-N, 2019 undefined. Reproducible, interactive, scalable and extensible microbiome data science using QIIME 2. nature.com [Internet]. [cited 2019 Oct 28]; Available from: https://www.nature.com/articles/s41587-019-0209-9

53. Caporaso JG, Kuczynski J, Stombaugh J, Bittinger K, Bushman FD, Costello EK. QIIME allows analysis of high-throughputcommunity sequencing data. Nat Methods [Internet]. 2010 [cited 2018 Apr 25];7. Available from: https://www.nature.com/articles/nmeth.f.303

54. Quast C, Pruesse E, Yilmaz P, … JG-N acids, 2012 undefined. The SILVA ribosomal RNA gene database project: improved data processing and web-based tools. academic.oup.com [Internet]. [cited 2019 Oct 28]; Available from: https://academic.oup.com/nar/article-abstract/41/D1/D590/1069277

55. Pedersen MW, Overballe-petersen S, Ermini L, Sarkissian C Der, Haile J, Hellstrom M, et al. Ancient and modern environmental DNA. … R … [Internet]. 2015; Available from: http://classic.rstb.royalsocietypublishing.org/content/370/1660/20130383.short

56. Ene A, Bosneaga A, Phys LG-RJ, 2010 undefined. Determination of heavy metals in soils using XRF technique. researchgate.net [Internet]. [cited 2019 Oct 28]; Available from: https://www.researchgate.net/profile/Antoaneta_Ene/publication/234076093_Determination_of_heavy_metals_in_soils_using_XRF_technique/links/02e7e5288bdbb82d58000000.pdf

57. Brown TA, Barnes IM. The current and future applications of ancient DNA in Quaternary science. J Quat Sci. 2015;30(2):144–53.

58. Dabney J, Meyer M, Pa S. Ancient DNA Damage. Cold Spring Harb Perspect Biol. 2013;5(7):1–7.

59. Taylor GM, Mays SA, Huggett JF. Ancient DNA (aDNA) studies of man and microbes: General similarities, specific differences. Int J Osteoarchaeol. 2010;20(6):747–51.

60. Willerslev E, Hansen AJ, Rønn R, Brand TB, Barnes I, Wiuf C, et al. Long-term persistence of bacterial DNA. Curr Biol. 2004;14(1):13–4.

61. Weyrich L, Dobney K, evolution AC-J of human, 2015 undefined. Ancient DNA analysis of dental calculus. Elsevier [Internet]. [cited 2018 Apr 25]; Available from: https://www.sciencedirect.com/science/article/pii/S0047248414002541

62. Young JM, Rawlence NJ, Weyrich LS, Cooper A. Limitations and recommendations for

successful DNA extraction from forensic soil samples: A review. Sci Justice [Internet]. 2014;54(3):238–44. Available from: http://dx.doi.org/10.1016/j.scijus.2014.02.006

63. Gugerli F, Parducci L, Petit RJ. Ancient plant DNA: Review and prospects. New Phytol. 2005;166(2):409–18.

64. Hebsgaard MB, Phillips MJ, Willerslev E. Geologically ancient DNA: Fact or artefact? Trends Microbiol. 2005;13(5):212–20.

65. Kuhry P. Palaeobotanical-palaeoecological studies of tropical high Andean peatbog sections (Cordillera Oriental, Colombia). J. Cramer; 1988. 241 p.

66. Sriskantharajah S, Fisher R, … DL-TBC, 2012 undefined. Stable carbon isotope signatures of methane from a Finnish subarctic wetland. Taylor Fr [Internet]. [cited 2019 Oct 28]; Available from: https://www.tandfonline.com/doi/abs/10.3402/tellusb.v64i0.18818

67. Allen JRL, Lamb AL, Dark P. Seasonality of δ ^{13}C and C/N ratios in modern and mid-Holocene sediments in the Severn Estuary Levels, SW Britain. The Holocene [Internet]. 2007 Jan 27 [cited 2019 Oct 28];17(1):139–44. Available from: http://journals.sagepub.com/doi/10.1177/0959683607073296

68. Metcalfe SE, Jones MD, Davies SJ, Noren A, MacKenzie A. Climate variability over the last two millennia in the North American Monsoon region, recorded in laminated lake sediments from Laguna de Juanacatlán, Mexico. The Holocene [Internet]. 2010 Dec 20 [cited 2019 Oct 28];20(8):1195–206. Available from: http://journals.sagepub.com/doi/10.1177/0959683610371994

69. Corella J, Brauer A, Mangili C, … VR-Q, 2012 undefined. The 1.5-ka varved record of Lake Montcortès (southern Pyrenees, NE Spain). cambridge.org [Internet]. [cited 2019 Oct 28]; Available from: https://www.cambridge.org/core/journals/quaternary-research/article/15ka-varved-record-of-lake-montcortes-southern-pyrenees-ne-spain/03E81724358CCF60A2B59BD1F5CCDBBD

70. Moreno A, Giralt S, Valero-Garcés B, Sáez A, Bao R, Prego R, et al. A 14 kyr record of the tropical Andes: The Lago Chungará sequence (18°S, northern Chilean Altiplano). Quat Int [Internet]. 2007 Feb 1 [cited 2019 Oct 28];161(1):4–21. Available from: https://www.sciencedirect.com/science/article/pii/S1040618206002461

71. Haug GH, Hughen KA, Sigman DM, Peterson LC, Röhl U. Southward Migration of the Intertropical Convergence Zone Through the Holocene. Science (80-). 2001;293(5533).

72. Conroy J, Overpeck J, Cole J, … TS-QS, 2008 undefined. Holocene changes in eastern tropical Pacific climate inferred from a Galápagos lake sediment record. Elsevier [Internet]. [cited 2019 Oct 28]; Available from: https://www.sciencedirect.com/science/article/pii/S0277379108000589

73. Naveed M, Herath L, Moldrup P, … EA-AS, 2016 undefined. Spatial variability of microbial richness and diversity and relationships with soil organic carbon, texture and structure across an agricultural field. Elsevier [Internet]. [cited 2019 Oct 28]; Available from: https://www.sciencedirect.com/science/article/pii/S092913931630066X

74. Key FM, Posth C, Krause J, Herbig A, Bos KI. Mining Metagenomic Data Sets for Ancient DNA: Recommended Protocols for Authentication. Trends Genet [Internet].

2017;33(8):508–20. Available from: http://dx.doi.org/10.1016/j.tig.2017.05.005

75.   Evans PN, Boyd JA, Leu AO, Woodcroft BJ, Parks DH, Hugenholtz P, et al. An evolving view of methane metabolism in the Archaea. Nat Rev Microbiol [Internet]. 2019 Apr 21 [cited 2019 Oct 28];17(4):219–32. Available from: http://www.nature.com/articles/s41579-018-0136-7

76.   Rooney-Varga JN, Giewat MW, Duddleston KN, Chanton JP, Hines ME. Links between archaeal community structure, vegetation type and methanogenic pathway in Alaskan peatlands. FEMS Microbiol Ecol [Internet]. 2007 May 1 [cited 2019 Oct 28];60(2):240–51. Available from: https://academic.oup.com/femsec/article-lookup/doi/10.1111/j.1574-6941.2007.00278.x

77.   Narrowe AB, Angle JC, Daly RA, Stefanik KC, Wrighton KC, Miller CS. High-resolution sequencing reveals unexplored archaeal diversity in freshwater wetland soils. Environ Microbiol [Internet]. 2017 Jun 1 [cited 2019 Oct 28];19(6):2192–209. Available from: http://doi.wiley.com/10.1111/1462-2920.13703

78.   Pazinato J, Paulo E, Mendes L, Diversity RV-, 2010 undefined. Molecular characterization of the archaeal community in an Amazonian wetland soil and culture-dependent isolation of methanogenic archaea. mdpi.com [Internet]. [cited 2019 Oct 28]; Available from: https://www.mdpi.com/1424-2818/2/7/1026

79.   Conrad R, Klose M, … PC-L and, 2010 undefined. Methanogenic pathway, 13C isotope fractionation, and archaeal community composition in the sediment of two clear-water lakes of Amazonia. Wiley Online Libr [Internet]. [cited 2019 Oct 28]; Available from: https://aslopubs.onlinelibrary.wiley.com/doi/abs/10.4319/lo.2010.55.2.0689

Supplementary Material

Supplementary Table 1. *Calibrated ages for every section of VERJON-1, including maximum, minimum, median and mean ages.*

DEPTH	MIN	MAX	MEDIAN	MEAN
0	-44	-5	-8	-11
1	-7	173	43	54
2	20	259	112	120
3	66	350	177	185
4	147	419	272	254
5	184	584	337	350
6	238	735	427	443
7	300	856	522	535
8	362	989	612	629
9	426	1113	708	725
10	494	1224	802	818
11	568	1352	896	913
12	639	1452	989	1003
13	704	1570	1084	1097

14	779	1670	1180	1192
15	858	1777	1276	1287
16	943	1881	1367	1380
17	1013	1981	1459	1471
18	1102	2078	1561	1569
19	1183	2193	1654	1662
20	1275	2295	1746	1756
21	1351	2389	1840	1850
22	1441	2489	1931	1943
23	1519	2578	2027	2034
24	1604	2685	2120	2127
25	1699	2781	2216	2221
26	1782	2872	2307	2314
27	1868	2962	2401	2408
28	1967	3050	2503	2502
29	2060	3146	2591	2596
30	2139	3237	2689	2691
31	2225	3334	2786	2783
32	2327	3410	2877	2876
33	2419	3501	2971	2969
34	2510	3591	3061	3059
35	2608	3685	3157	3156
36	2703	3784	3254	3250
37	2797	3864	3346	3339
38	2876	3940	3434	3430
39	2980	4014	3531	3523
40	3084	4092	3623	3615
41	3168	4173	3720	3709
42	3276	4248	3818	3804
43	3380	4328	3913	3898
44	3477	4407	4005	3993
45	3583	4488	4107	4089
46	3686	4565	4199	4180
47	3792	4643	4298	4275
48	3908	4718	4392	4371
49	4024	4781	4487	4465
50	4140	4848	4583	4559
51	4256	4913	4675	4650
52	4369	4974	4769	4745
53	4481	5037	4861	4840
54	4584	5101	4936	4930
55	4642	5165	4992	4978
56	4696	5228	5036	5026

57	4752	5279	5082	5072
58	4816	5333	5128	5119
59	4871	5386	5174	5166
60	4923	5436	5221	5213
61	4975	5488	5268	5261
62	5026	5537	5316	5308
63	5084	5584	5362	5356
64	5135	5638	5409	5405
65	5185	5683	5456	5452
66	5230	5726	5506	5500
67	5289	5776	5552	5546
68	5333	5820	5598	5593
69	5382	5864	5648	5641
70	5437	5906	5694	5689
71	5493	5948	5742	5737
72	5548	5988	5789	5784
73	5607	6029	5840	5833
74	5660	6070	5886	5880
75	5716	6104	5934	5928
76	5770	6143	5983	5976
77	5830	6180	6030	6024
78	5891	6213	6079	6071
79	5953	6246	6126	6119
80	6023	6277	6174	6167
81	6089	6306	6217	6213
82	6193	6356	6269	6261
83	6221	6448	6308	6313
84	6248	6528	6358	6366
85	6280	6602	6411	6419
86	6313	6674	6462	6470
87	6350	6751	6512	6521
88	6388	6815	6565	6574
89	6425	6886	6618	6627
90	6463	6952	6673	6680
91	6496	7013	6723	6732
92	6542	7083	6776	6785
93	6582	7152	6829	6838
94	6623	7213	6879	6890
95	6668	7279	6933	6942
96	6706	7342	6986	6995
97	6752	7409	7038	7049
98	6795	7472	7091	7101
99	6836	7530	7146	7153

100	6883	7580	7198	7204
101	6921	7635	7245	7256
102	6969	7690	7298	7307
103	7014	7753	7351	7359
104	7059	7805	7404	7413
105	7107	7865	7457	7465
106	7151	7920	7509	7516
107	7189	7979	7561	7568
108	7232	8044	7616	7620
109	7278	8096	7667	7672
110	7328	8153	7717	7723
111	7372	8209	7768	7774
112	7413	8266	7819	7826
113	7463	8323	7873	7879
114	7507	8379	7920	7929
115	7557	8436	7971	7981
116	7605	8497	8026	8034
117	7657	8544	8079	8087
118	7699	8593	8131	8139
119	7755	8654	8183	8192
120	7799	8721	8238	8246
121	7840	8773	8291	8298
122	7890	8828	8341	8351
123	7941	8885	8395	8403
124	7993	8940	8448	8455
125	8038	8997	8500	8507
126	8091	9055	8552	8559
127	8139	9110	8607	8611
128	8184	9167	8659	8663
129	8239	9221	8710	8715
130	8286	9276	8761	8767
131	8336	9329	8814	8818
132	8384	9380	8864	8870
133	8434	9440	8918	8921